

## SEARCHING FOR TRAJECTORIES TO ASTEROIDS USING SOLAR SAILS

Cristiano F. de Melo,<sup>\*</sup> Antonio F. B. A. Prado,<sup>†</sup>  
Lucas G. Meireles<sup>‡</sup> and Maria C. Pereira<sup>§</sup>

This paper describes trajectories to asteroids using solar sails as a propulsion system. Asteroids are an interesting target for space exploration for scientific and technological missions, but also present potential collisions to the Earth to be avoided. In this work the dynamics of the solar sail is described and the equations are presented. Several trajectories for a spacecraft to reach an asteroid are shown, with the goal of mapping trajectories for a mission designer to choose from. The main elements involved in the trajectory are measured, like the velocities, angle of collision, etc. Using those data any type of mission can be designed.

### INTRODUCTION

Exploration of comets and asteroids have arisen interest of aerospace community, for scientific purposes, because they provide important information regarding the origin of planets and life<sup>1</sup>. Missions aiming comets and asteroids for scientific exploration have been performed, as Vega mission to comet Halley and Rosetta Mission to comet 67/P Churyumov-Gerasimenko<sup>2</sup>. Interest also arises for practical reasons, such as potential collision with each other or our planet. In this context, Near Earth Asteroids (NEAs) can be a threat to Earth and human kind. Another source of interest for future exploration is space mining, considering that asteroids are rich in rare metals and mineral resources<sup>1,3</sup>, or redirecting asteroids for future exploration<sup>4</sup>.

Meanwhile, another subject that has been studied is the use of solar radiation pressure as a propulsion method. The solar radiation pressure is a well modeled and studied effect, being considered in most cases a disturbance acting on the spacecraft. Nevertheless, for the last years it has been studied as a propulsion method used in the so-called solar sails, minimizing the onboard fuel needed to fulfill a mission. Even though the early concept was mentioned for the first time in the 20<sup>th</sup> century by Tsiolkovsky and Tsander and first studies were presented in the 60's<sup>5</sup>, for many decades its use was not possible, because the materials technology was not well developed. Re-

---

<sup>\*</sup> PhD, Department of Mechanical Engineering, Federal University of Minas Gerais, Brazil.  
E-mail: cristiano.fiorilo@demec.ufmg.br.

<sup>†</sup> PhD, Dean of Graduate Studies, National Institute for Space Research, Brazil. E-mail: antonio.prado@inpe.br.

<sup>‡</sup> B.E., Space Mechanics and Control Division, National Institute for Space Research, Brazil.  
E-mail: meireleslg@gmail.com.

<sup>§</sup> PhD, Department of Mechanical Engineering, Federal University of Minas Gerais, Brazil.  
E-mail: cecilia@demec.ufmg.br.

cent technologies, however, have made it possible to make use of solar sails in real missions, such as IKAROS in 2010<sup>6</sup>.

The idea of using a spacecraft equipped with a solar sail, also called a sailcraft, to rendezvous with a NEAs is not recent, being addressed for sample return missions<sup>7,8</sup>. It was shown then that it is possible to perform multiple rendezvous with NEAs, returning to Earth with no other propulsion method within reasonable mission duration times, even with moderate-performance sails.

In the present paper it is shown several trajectories for a spacecraft to reach an asteroid using a solar sail as a propulsion system. The idea is to map the trajectories showing the possibilities for a mission designer. The main elements involved in the trajectory are measured, like the relative velocity between the asteroid and the spacecraft, the angle between those velocities, the flight time from the Earth to the asteroid, the initial true anomaly of the spacecraft at departure, the true anomaly of the asteroid at point of encounter and the sail azimuth angle. In the situations where an impact occur, it is also measured the asteroid velocity, the specific angular momentum, and the semi-major axis and eccentricity of the orbit, as well as the deviation of the perihelion of the orbit of the asteroid. Using those data any type of mission can be designed.

## SOLAR SAILING

The main limitation for a mission duration is the onboard fuel loaded by the satellite. Since the main forms of propulsion rely on a reaction mass accelerated to the opposite direction of the desired movement, once the fuel is totally consumed the satellite becomes unmaneuverable. Solar sails present an alternative for such a problem, considering that it uses a natural resource largely available in the solar system: solar radiation.

Since solar sails are not limited by a finite reaction mass, they can provide a continuous acceleration, limited by the aging of the film. For the phenomenon to be expressive enough to be used as a propulsion system, the area of the sail must be large, such that it collects a large number of photons and light, in order to generate a significant acceleration. The material of the sail must be very reflexive<sup>5</sup> as well, since a perfect reflector gets twice the pressure, because momentum switches direction, instead of simply being reflected<sup>9</sup>. Those conditions will provide a small, but continuous acceleration to the sail, allowing considerable speeds to be achieved.

Three basic configurations of flat solar sails are usually found in literature<sup>10</sup>, as shown in Figure 1. Three of them, the square sail, the spinning disk and the heliogyro, present advantages and disadvantages in terms of controllability, packaging, deployment, mass, cost, among others. The selection of the configuration is a complex problem. The square sail is the most studied one, so it is most likely to be used for near term sail missions.

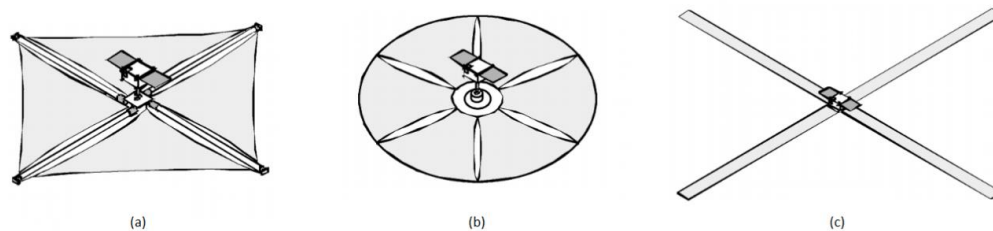


Figure 1. Common configurations of a solar sail. (a) Square solar sail; (b) Spinning disk; (c) Heliogyro<sup>10</sup>

The study, design and fabrication of a solar sail use multidisciplinary concepts. Solar radiation pressure strikes the surface of the sail, being partially reflected, absorbed and thermally reemitted. In this process, solar radiation transfers linear momentum to the sail structure. The resulting force can then be used to maneuver the vehicle, using control laws that allow a proper operation of the sail<sup>11</sup>.

### Physical Phenomenon

Solar radiation is a well modeled effect regarding intensity and spectrum, being isotropic. The Sun can then be considered as an uniformly luminous disk, allowing it to be modeled as a plain area irradiating uniformly to space<sup>12</sup>. The phenomena involved in solar radiation pressure can be analyzed either considering quantum mechanics or electromagnetism. Both theories get the same results<sup>5</sup>, and so here the quantum approach is presented.

In order to understand well the effect of solar radiation pressure, one must consider both quantum mechanics and special relativity<sup>5</sup>. The photons of the solar radiation transport energy proportional to their frequencies, as stated in Planck's law:

$$E = h\nu \quad (1)$$

where  $E$  is the energy of the photon and  $h$  is Planck's constant. Also, the energy can be described by mass-energy equivalence, and, since the photon has no rest mass:

$$E = pc \quad (2)$$

where  $p$  is the momentum of the photon and  $c$  is the speed of light. From Equations (1) and (2), the momentum is given by:

$$p = \frac{h\nu}{c} \quad (3)$$

Let  $W$  be the energy flux at a distance  $r$  from the Sun. Considering  $L_s$  the solar luminosity,  $W$  can be written as:

$$W = \frac{L_s}{4\pi^2} \quad (4)$$

The amount of energy  $\Delta E$  across a surface of area  $A$  in a time period  $\Delta t$  is given by:

$$\Delta E = WA\Delta t \quad (5)$$

From Equation (2), this energy transports a momentum  $\Delta p$ :

$$\Delta p = \frac{\Delta E}{c} \quad (6)$$

and, since the pressure is defined as the momentum transported through a surface per unit area per unit time, one gets:

$$P = \frac{1}{A} \left( \frac{\Delta p}{\Delta t} \right) \quad (7)$$

From Equations (5) and (7), the solar radiation pressure can be expressed as:

$$P = \frac{W}{c} \quad (8)$$

The pressure exerted on a perfectly reflecting solar sail at 1 AU (astronomical unit, the average Sun-Earth distance) is then  $9.12 \times 10^{-6} \text{ Nm}^{-2}$ . During a year it can vary up to 3.5%, but as an average this value is considered to be correct<sup>5</sup>. This pressure causes forces and torques acting on the sail, i.e., the momentum transfer causing mechanical forces and associated torques, which are not neglectable<sup>12</sup>.

Considering that light can be absorbed and reflected, either specularly and diffusely, all those effects will count to the dynamics<sup>5,9,11</sup>. Specularly reflected light causes a force normal to its surface. Absorbed light transfers momentum to the sail in the same direction of the incidence light. This light is emitted by both sail sides, determining not only the sail temperature but also generating a thrust. If the emission coefficient is denoted by  $\chi$  and  $\epsilon$  is the temperature-dependent emissivity, and letting  $b$  and  $f$  refer to the back and front side of the sail, respectively, the net thrust is proportional to the absorbed radiation by the factor  $\kappa$ :

$$\kappa \equiv \frac{\chi_f \epsilon_f(T) - \chi_b \epsilon_b(T)}{\epsilon_f(T) + \epsilon_b(T)} \quad (9)$$

Regarding the diffusely reflected light, it is considered that the tangent components of the reflected light rays cancel each other, resulting in a force normal to the surface<sup>9,11</sup>.

### Mathematical Solar Sail Force Model

The thrust caused by electromagnetic radiation pressure can be used for the dynamic model of the sailcraft<sup>5,11</sup>. For the correct analysis, the frames of reference must be well defined as follows.

*Frames of reference.* Let HIF be the heliocentric inertial frame and HOF be the sailcraft orbital frame. HIF is centered at the Sun's barycenter<sup>11</sup>, and their relation can be seen in Figure 2.

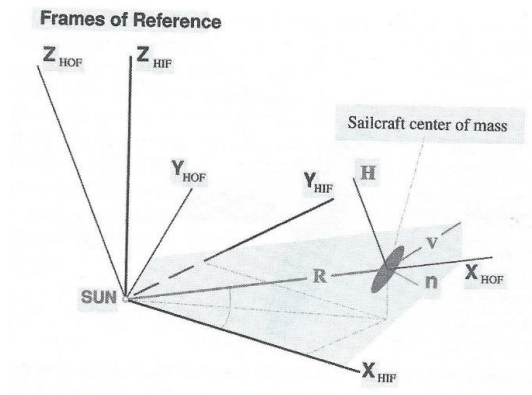


Figure 2. Frames of Reference<sup>11</sup>

In Figure 2,  $\mathbf{R}$  and  $\mathbf{V}$  denote the vectors for position and velocity of the sailcraft. Note that in case the sailcraft's movement is retrograde,  $\mathbf{Z}_{\text{HOF}}$  points to the direction opposite to the one shown in the figure. Figure 3 shows a flat sail oriented in HOF and the resulting thrust  $\mathbf{T}$ . The matrix that transforms a vector presented in HOF into a corresponding vector in HIF is given by:

$$\Xi = (\mathbf{r} \quad \mathbf{r} \times \mathbf{h} \quad \mathbf{h}) \quad (10)$$

where  $\mathbf{r}$  is position vector of the sailcraft and  $\mathbf{h}$  is the angular momentum.

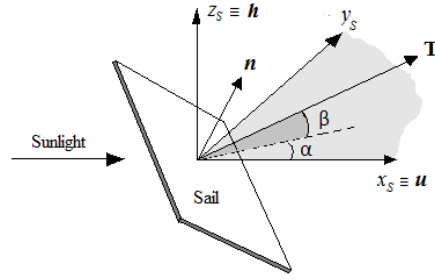


Figure 3. Thrust of a sailcraft.<sup>11</sup>

*Lightness vector.* The thrust acceleration of the sail normalized to the local solar gravitational acceleration is called Lightness. Considering that the sail is far enough from the Sun, in HOF, one gets<sup>11</sup>:

$$\mathbf{A}^{HOF} = \mathbf{g}_\odot \mathbf{L} = \left( \frac{GM_\odot}{R^2} \right) \left( \frac{\sigma_c}{2\sigma} \right) \{ n_x [(2r_{spec}n_x + \chi_f r_{diff} + \kappa a)\mathbf{n} + (a + r_{diff})\mathbf{u}] \} = B\Gamma \quad (11)$$

$$\mathbf{L} = [(2r_{spec}n_x + \chi_f r_{diff} + \kappa a)\mathbf{n} + (a + r_{diff})\mathbf{u}] \quad (12)$$

where:

$$B = \left( \frac{GM_\odot}{R^2} \right) \left( \frac{\sigma_c}{2\sigma} \right) n_x$$

$$\sigma_c = 2 \frac{I_{1AU}}{c g_{1AU}} \approx 1.5368 g/m^2$$

$$\sigma = m/S$$

and:

$g_\odot$  is the local solar gravitational acceleration;  $\mathbf{L}=(l_x l_y l_z)$  is the lightness vector;  $G$  is the gravitational constant;  $M_\odot$  is the mass of the Sun;  $\mathbf{R}=(x y z)$  is the position of the sailcraft with respect to the Sun, being  $R$  its magnitude;  $\sigma_c$  is the critical loading;  $\sigma$  is the actual loading, mass  $m$  divided by effective sail area  $S$ ;  $c$  is the speed of light;  $\mathbf{n}=(n_x n_y n_z)$  is the unit vector normal to the sail;  $r_{spec}$  is the specularly reflectance of the frontside of the sail;  $r_{diff}$  is the diffusely reflectance of the frontside of the sail;  $a$  is the absorptance of the frontside of the sail;  $\mathbf{u}$  is the direction of the Sun, or  $X_{HOF}$ ;  $I_{1AU}$  is the intensity of the solar radiation at 1 AU ( $=1366W/m^2$ ).

The acceleration in HIF is, then, given by Equations (13) and (14):

$$\mathbf{A}^{HIF} = \Xi \mathbf{A}^{HOF} = g_\odot (\mathbf{r} \quad \mathbf{r} \times \mathbf{h} \quad \mathbf{h}) \begin{pmatrix} l_x \\ l_y \\ l_z \end{pmatrix} = \frac{g_{1AU}}{R^2} (l_x r \quad l_y |\mathbf{r} \times \mathbf{h}| \quad l_z h) \quad (13)$$

$$\mathbf{A}^{HIF} = \frac{GM_{\odot}}{R^2} \left\{ \begin{array}{l} \frac{l_x}{R}x + \frac{l_y}{hR}[z(zv_x - xv_z) - y(xv_y - yv_x)] + \frac{l_z}{h}(yv_z - zv_y) \\ \frac{l_x}{R}y + \frac{l_y}{hR}[x(xv_y - yv_x) - z(yv_z - zv_y)] + \frac{l_z}{h}(zv_x - xv_z) \\ \frac{l_x}{R}z + \frac{l_y}{hR}[y(yv_z - zv_y) - x(zv_x - xv_z)] + \frac{l_z}{h}(xv_y - yv_x) \end{array} \right\} \quad (14)$$

where

$\mathbf{h} = (h_x, h_y, h_z)$  is the angular momentum of the orbit of the sailcraft, with  $h$  being its magnitude

$\mathbf{v} = (v_x, v_y, v_z)$  is the velocity of the sailcraft

The lightness vector can be expressed in terms of the angles  $\alpha$ ,  $\delta$ , defined in Figure (3):

$$\mathbf{L} = \left\{ \begin{array}{l} \left( \frac{1}{2} \frac{\sigma_c}{\sigma} \right) [2r_{spec} \cos^3 \delta \cos^3 \alpha + (\chi_f r_{diff} + \kappa a_f) \cos^2 \delta \cos^2 \alpha] + \\ \quad + (a_f + r_{diff}) \cos \delta \cos \alpha \\ \left( \frac{1}{2} \frac{\sigma_c}{\sigma} \right) [2r_{spec} \cos^3 \delta \cos^2 \alpha \sin \alpha + (\chi_f r_{diff} + \kappa a_f) \cos^2 \delta \cos \alpha \sin \alpha] \\ \left( \frac{1}{2} \frac{\sigma_c}{\sigma} \right) [2r_{spec} \cos^2 \delta \cos^2 \alpha \sin \delta + (\chi_f r_{diff} + \kappa a_f) \cos \delta \cos \alpha \sin \delta] \end{array} \right\} \quad (15)$$

**Table 1. Optical properties of the sailcraft<sup>5</sup>.**

	$r$	$S$	$\varepsilon_f$	$\varepsilon_b$	$b_f$	$b_b$
Ideal sail	1	1	0	0	2/3	2/3
Square sail	0.88	0.94	0.05	0.55	0.79	0.55
Heliogyro	0.88	0.94	0.05	0.55	0.79	0.55

The optical properties considered in the equations were obtained at JPL/NASA and are presented in Table 1<sup>5</sup> for two of the three basic configurations of the solar sail, compared to the ideal case.

### Solar Sail Orbital Dynamics

The orbital dynamics of a solar sail, provided its continuous-low-thrust propulsion, is similar to other systems, as an electric propulsion, for example. The main difference relies on the fact that the control angle is limited to  $90^\circ$  with respect to the Sun's direction<sup>5</sup>. A wide range of orbits can be explored by the sailcraft, from Sun-centered orbits (conic sections, circular, elliptical, rectilinear, escape, logarithmic spiral, among others) to planet-centered ones and minimum time trajectories. The main factor that allows each of those orbits to be achieved is the lightness number, that depends essentially on the material of the film of the sail.

Displaced non-Keplerian Sun-centered orbits can also be achieved, grouped into three families of orbits. Type I orbits have the period to be fixed for all values of orbit radius and displacement.

Type II family refers to orbits which period is chosen to be the same one of a Keplerian orbit with radius equals to the Sun-sail distance. Type III orbits are obtained to minimize the solar sail lightness number, leaving the orbit period as a free parameter<sup>5</sup>. Other cases can be obtained as well, choosing the orbital period appropriately. Displaced non-Keplerian planet-centered orbits are also investigated, and the three families can be found as well. Types I and III are defined in the same way than the Sun-centered ones, and Type 2 is defined with the period proportional to the distance to the Sun, synchronous with the Keplerian orbit. The stability and controllability of those orbits show that there exist some regions where the orbits are both stable and controllable. Equilibrium solutions in the Earth-Sun system can be found as well, and also depend on the lightness number. Those equilibrium points are usually unstable, but still controllable.

## RESULTS

The present session will show a series of simulations that can map trajectories for a sailcraft going from the Earth to an asteroid.

### Using a Sailcraft with a mass-area ratio of 5.27 g/m<sup>2</sup>

The objective is to evaluate the behavior of a sailcraft equipped with a solar sail with a mass-area ratio of 5.27 g/m<sup>2</sup> in an interception missions to follow or deviate an asteroid with a mass of 10<sup>7</sup> kg. Having this goal in mind, we analyze the time of flight for interception, the relative velocity between the sailcraft and the target asteroid and the angle between their velocities (flight direction) at the time of the interception and, in the case of impact, the deviation generated.

The total mass-area ratio of the sailcraft, 5.27 g/m<sup>2</sup>, can be considered small. The basic design of this sailcraft consists in a square sail with a total mass of 20 kg, distributed between the sail, with a mass of 5 kg (mass-area ratio of the sail of 1.32g/m<sup>2</sup>), its structure (cables, sensors, etc.) with a mass of 10 kg, and, as a payload, a 3U cubsat with 5 kg. The total area required is therefore of the order of 3,795 m<sup>2</sup>. The target asteroid used for this simulation is hypothetical, with a mass of 10<sup>7</sup> kg, semi-major axis of 2 A.U. and eccentricity of 0.5. The inclination, ascending node and argument of the perihelion were considered zero.

In addition to the asteroid and the sailcraft, the masses of the Sun, the Earth, the Moon, Venus, Mars and Jupiter were considered, all of them assumed to be in circular orbits and distributed randomly in space, simply by assigning values to the initial true anomalies of each body. The initial true anomalies used were: 50° for the Earth, 120° for the Moon, 100° for Venus, 250° for Mars and 300° for Jupiter. For the asteroid, the initial true anomaly considered was zero. For the sailcraft, eight starting positions were considered, with respect to the Earth, all of them in a circular orbit equal to 930,000 km, which is roughly the value of the radius of the sphere of influence of the Earth. The positions are then defined by the initial true anomalies of the sailcraft,  $f_{SC}$ , relative to the Earth, that is,  $f_{SC} = 0, 45, 90, 135, 180, 225, 270,$  and 315 degrees.

The azimuth angle of the sail  $\alpha$  ranged from -85 to 85 degrees, in steps of 1 degree. However, once the propagation of an orbit begins, the value of  $\alpha$  remains constant, which assumes the existence of a control device that keeps it constant. The elevation  $\beta$  was considered zero, which means a planar problem. The quantities  $\alpha$  and  $\beta$  can be seen in Figure 4, as well as the direction of the thrust on a square sail. When  $\beta = 0$ , the thrust is coplanar with the orbital plane of the sailcraft. Since  $\alpha$  is not zero, there will be radial and tangential components that can accelerate or decelerate the trajectory of the sailcraft. During the simulations, 360 positions for possible encounters on the orbit of the asteroid were considered, in steps of 1°, with each position defined by the true

anomaly of the asteroid  $f_A$ . Thus, for each of the 360 possible values for  $f_A$ , 170 possible values of  $\alpha$  were tested from each of the initial 8 positions on the initial orbit of the sailcraft defined by  $f_{SC}$ . It means that 489,600 trajectories were propagated. The propagation time of each orbit was 5 years. Whenever the trajectory of a sailcraft approaches less than 10 km from the position occupied by the asteroid, an encounter is assumed to occur and it is recorded, as well as the values of the relative velocity between the asteroid and the sailcraft ( $\Delta V$ ), the angle between the velocities ( $\Delta\theta$ ), the flight time ( $T_{of}$ ), the initial true anomaly of the sailcraft at departure ( $f_{SC}$ ), the true anomaly of the asteroid at encounter ( $f_A$ ) and the sail azimuth angle ( $\alpha$ ). In the case of the direct impact analysis (considered to be an inelastic collision) between the sailcraft and the asteroid, the asteroid velocity ( $\Delta V_A$ ), the specific angular momentum ( $\Delta H_A$ ), the semi-major axis ( $\Delta a_A$ ), the eccentricity of the orbit ( $\Delta e_A$ ) and the deviation in the perihelion ( $\Delta R_{pA}$ ) are also measured to show the effects of the collision in the orbit of the asteroid. No significant variations were observed in the values of the inclination, ascending node and perihelion argument of the orbit of the asteroid, although those quantities were also measured. Eight encounters (solutions) were found.

The results show that the lowest relative velocities between the sailcraft and the asteroid ( $\Delta V$ ) occur, in general, for true anomalies of the asteroid ( $f_A$ ) in the 3rd and 4th quadrants, which are the regions where the angle ( $\Delta\theta$ ) between their velocities are small. As an example, for the smallest variation of velocity found (solution 5, shown in Fig. 4), we have  $f_A = 222^\circ$ ,  $\Delta V = 7.035$  km/s, and  $\Delta\theta = 23.061^\circ$ . For the second best solution in this point (solution 10, shown in Fig. 5), we have  $f_A = 353^\circ$ ,  $\Delta V = 7.242$  km/s and  $\Delta\theta = 2.027^\circ$ . However,  $\Delta V > 10$  km/s are also found for  $f_A > 180^\circ$ , and no encounter with  $\Delta V < 10$  km/s was found for  $f_A < 180^\circ$ .

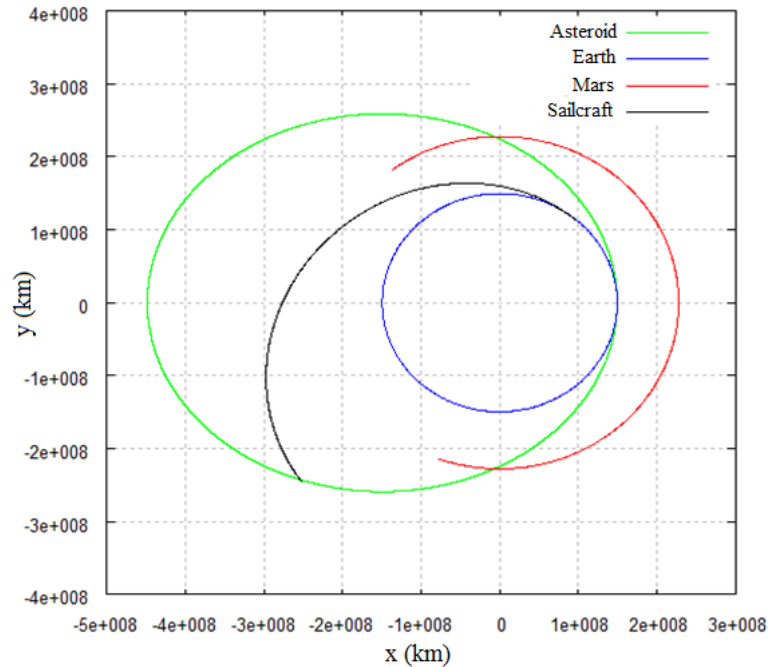
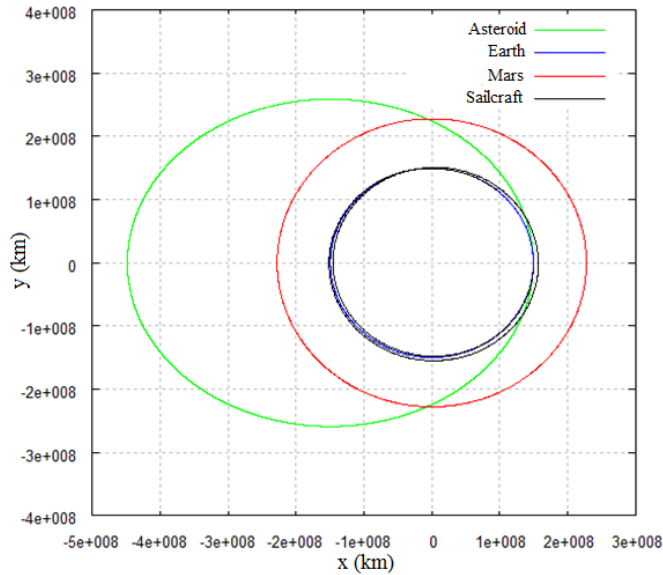
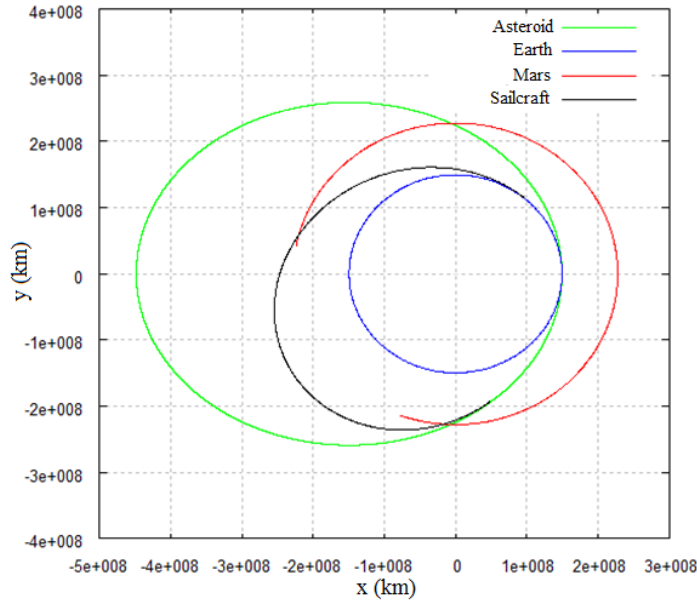


Figure 4. Solution 5.



**Figure 6. Solution 10.**

In the analysis of the impact and deviation, the best results also generally occur for values of  $f_A$  in the 3th and 4th quadrants, if the encounter does not occur very close to the perihelion. However, a solution was found with  $f_A = 68^\circ$ ,  $\Delta\theta = 25.787^\circ$  and  $\Delta R_{PA} = 67.578$  km, which corresponds to the second best solution from the point of view of deviation. Following the analysis, comparing solution 8 (best result for deviation with  $\Delta V = 8.107$  km/s,  $\Delta\theta = 0.159^\circ$  and  $\Delta R_{PA} = 81.030$  km, shown in Fig. 6) with solution 10 (worst result for deviation with  $\Delta V = 7.242$  km/s,  $\Delta\theta = 2.027^\circ$  and  $\Delta R_{PA} = 1.624$  km, shown in Fig. 5), although both solutions occur in the 4th quadrant, in the solution 10 the encounter occurred very close to the perihelion of the orbit of the asteroid, where its velocity is high. Therefore, even for a small  $\Delta\theta$ , the velocity variation of the asteroid is small and does not alter the perihelion of the asteroid. Regarding the attitude of the sail, defined by  $\alpha$ , it was possible to find the smallest  $\Delta V$  for both small ( $-5^\circ$ ,  $-1^\circ$ ,  $3^\circ$  and  $9^\circ$ ) and high values ( $-83^\circ$ ). In this way, it is concluded that the most important is to ensure an asteroid approach with the smallest possible angle ( $\Delta\theta$ ) between its velocities and as far away as possible from its aphelion.



**Figure 7. Solution 8.**

All the solutions found are listed next.

Solution 1:  $\Delta V = 10.912$  km/s,  $\Delta\theta = 18.869^\circ$ ,  $T_{of} = 855.654$  days,  $f_{SC} = 45^\circ$ ,  $f_A = 62^\circ$ ,  $\alpha = 81^\circ$ ,  $\Delta V_A = 2.182 \times 10^{-5}$  km/s,  $\Delta H_A = 1245.42$  km<sup>2</sup>/s,  $\Delta a_A = -577.82$  km,  $\Delta e_A = -1.2078 \times 10^{-6}$  and  $\Delta R_{PA} = 42.017$  km.

Solution 2:  $\Delta V = 10.119$  km/s,  $\Delta\theta = 17.618^\circ$ ,  $T_{of} = 1731.770$  days,  $f_{SC} = 225^\circ$ ,  $f_A = 65^\circ$ ,  $\alpha = 83^\circ$ ,  $\Delta V_A = 2.023 \times 10^{-5}$  km/s,  $\Delta H_A = 1092.669$  km<sup>2</sup>/s,  $\Delta a_A = -522.28$  km,  $\Delta e_A = -8.220 \times 10^{-7}$  and  $\Delta R_{PA} = 40.697$  km.

Solution 3:  $\Delta V = 13.609$  km/s,  $\Delta\theta = 25.787^\circ$ ,  $T_{of} = 1751.24$  days,  $f_{SC} = 135^\circ$ ,  $f_A = 68^\circ$ ,  $\alpha = 83^\circ$ ,  $\Delta V_A = 2.721 \times 10^{-5}$  km/s,  $\Delta H_A = 1092.711$  km<sup>2</sup>/s,  $\Delta a_A = -629.83$  km,  $\Delta e_A = -1.250 \times 10^{-6}$  and  $\Delta R_{PA} = 65.578$  km.

Solution 4:  $\Delta V = 15.047$  km/s,  $\Delta\theta = 60.756^\circ$ ,  $T_{of} = 1751.24$  days,  $f_{SC} = 45^\circ$ ,  $f_A = 208^\circ$ ,  $\alpha = 9^\circ$ ,  $\Delta V_A = 3.010 \times 10^{-5}$  km/s,  $\Delta H_A = 1397.8865$  km<sup>2</sup>/s,  $\Delta a_A = -293.99$  km,  $\Delta e_A = -2.884 \times 10^{-7}$  and  $\Delta R_{PA} = 41.479$  km.

Solution 5:  $\Delta V = 7.035$  km/s,  $\Delta\theta = 23.061^\circ$ ,  $T_{of} = 453.07$  days,  $f_{SC} = 270^\circ$ ,  $f_A = 222^\circ$ ,  $\alpha = 3^\circ$ ,  $\Delta V_A = 1.462 \times 10^{-5}$  km/s,  $\Delta H_A = 1528.5562$  km<sup>2</sup>/s,  $\Delta a_A = -241.62$  km,  $\Delta e_A = -2.774 \times 10^{-7}$  and  $\Delta R_{PA} = 65.321$  km.

Solution 6:  $\Delta V = 15.664$  km/s,  $\Delta\theta = 56.007^\circ$ ,  $T_{of} = 341.10$  days,  $f_{SC} = 135^\circ$ ,  $f_A = 224^\circ$ ,  $\alpha = 9^\circ$ ,  $\Delta V_A = 3.134 \times 10^{-5}$  km/s,  $\Delta H_A = 1370.8735$  km<sup>2</sup>/s,  $\Delta a_A = -436$  km,  $\Delta e_A = -6.945 \times 10^{-7}$  and  $\Delta R_{PA} = 3.647$  km.

Solution 7:  $\Delta V = 10.232$  km/s,  $\Delta\theta = 21.998^\circ$ ,  $T_{of} = 449.20$  days,  $f_{SC} = 225^\circ$ ,  $f_A = 249^\circ$ ,  $\alpha = -3^\circ$ ,  $\Delta V_A = 2.047 \times 10^{-5}$  km/s,  $\Delta H_A = 2392.2707$  km<sup>2</sup>/s,  $\Delta a_A = -519.02$  km,  $\Delta e_A = -5.603 \times 10^{-7}$  and  $\Delta R_{PA} = 67.013$  km.

Solution 8:  $\Delta V = 8.107$  km/s,  $\Delta\theta = 0.159^\circ$ ,  $Tof = 534.13$  days,  $f_{SC} = 90^\circ$ ,  $f_A = 285^\circ$ ,  $\alpha = -5^\circ$ ,  $\Delta V_A = 1.622 \times 10^{-5}$  km/s,  $\Delta H_A = 2971.4276$  km<sup>2</sup>/s,  $\Delta a_A = -653.50$  km,  $\Delta e_A = -8.161 \times 10^{-7}$  and  $\Delta R_{PA} = 81.030$  km.

Solution 9:  $\Delta V = 12.663$  km/s,  $\Delta\theta = 18.731^\circ$ ,  $Tof = 1662.38$  days,  $f_{SC} = 0^\circ$ ,  $f_A = 342^\circ$ ,  $\alpha = -1^\circ$ ,  $\Delta V_A = 2.534 \times 10^{-5}$  km/s,  $\Delta H_A = 2883.7025$  km<sup>2</sup>/s,  $\Delta a_A = -832.94$  km,  $\Delta e_A = -1.064 \times 10^{-6}$  and  $\Delta R_{PA} = 28.954$  km.

Solution 10:  $\Delta V = 7.242$  km/s,  $\Delta\theta = 2.027^\circ$ ,  $Tof = 688.46$  days,  $f_{SC} = 90^\circ$ ,  $f_A = 353^\circ$ ,  $\alpha = -83^\circ$ ,  $\Delta V_A = 1.448 \times 10^{-5}$  km/s,  $\Delta H_A = 2160.6222$  km<sup>2</sup>/s,  $\Delta a_A = -704.36$  km,  $\Delta e_A = -1.1471 \times 10^{-6}$  and  $\Delta R_{PA} = 1.624$  km.

### Using a Sailcraft with a mass-area ratio of 53.46 g/m<sup>2</sup>

We repeat the same search mechanism shown in the previous section, however, a sailcraft with a mass-area ratio (more realistic) of 53.46 g/m<sup>2</sup> and an asteroid with a mass of  $2 \times 10^9$  kg were considered. The analyses also took into account the time of flight for interception (Tof), the relative velocity between the sailcraft and the target asteroid ( $\Delta V$ ) and the angle between their velocities ( $\Delta\theta$ ) at the time of the interception and, in the case of impact, the deviation generated ( $\Delta R_{PA}$ ).

Taking into account recent advances pointed out in the literature (Vulpetti et al., 2015, Macdonald, 2014), a sailcraft equipped with a Sail with mass-area ratio of 5.2 g/m<sup>2</sup> and 10,000 m<sup>2</sup> was considered, therefore, with a mass of 52 kg. The Sail structure (cables, sensors, etc.) has a mass of 357.6 kg, and, as a payload, a structure with a mass of 115 kg in the central part of the sailcraft. The payload can be composed of scientific instruments or a kinetic impactor of 100 kg (driven by a spring or a small retrorocket) in the case of a deviation mission. Thus, the total mass of the sailcraft is 534.6 kg.

Another hypothetical target asteroid was also considered in the simulations. However, with semi-major axis of 295,917,661.9 km, eccentricity of 0.50180, inclination null, ascending node of 214.41 degrees, argument of the perihelion of 179.17 degrees and mass of  $2 \times 10^9$  kg. In this way, we have a target with a semi-major axis and eccentricity similar to the asteroid of the first simulations set, but with ascending node and argument of the perihelion non-zero.

The initial conditions of the other bodies (Sun, Earth, Moon, Venus, Mars and Jupiter) correspond to the ephemerides of December 31, 2025. The propagation time of each orbit was 10 years, instead of 5.

The results show a good number of encounters. In Figure 8, it is possible to see the options of encounters as a function of the true anomaly of the asteroid at the encounter point (8.a), and the time of flight (8.b). The trajectories with the smallest  $\Delta V = 2.842$  km/s,  $\Delta\theta = 1.543^\circ$ ,  $\Delta R_{PA} = 102$  km and time of flight of 2780.76 days, and the fastest transfer with time of flight of 205.79 days,  $\Delta V = 8.334$  km/s,  $\Delta\theta = 11.573^\circ$ ,  $\Delta R_{PA} = 117$  km are in the Figure 9.a and 9.b, respectively.

The simulations considering a sailcraft with mass-area 53.46 g/cm<sup>2</sup> present better interception options with small relative velocity between the sailcraft and asteroid than the simulations of the previous section. But the results for the impact do not present significant deviations for the two cases.

Variations in attitude of the sailcraft ( $\alpha$ ) during the transfer can accelerate or decelerate it to optimize the relative velocity ( $\Delta V$ ) to follow the target, or deviate it. However, the simulations shown here point to the real possibility of future applications for asteroid interception with sailcraft.

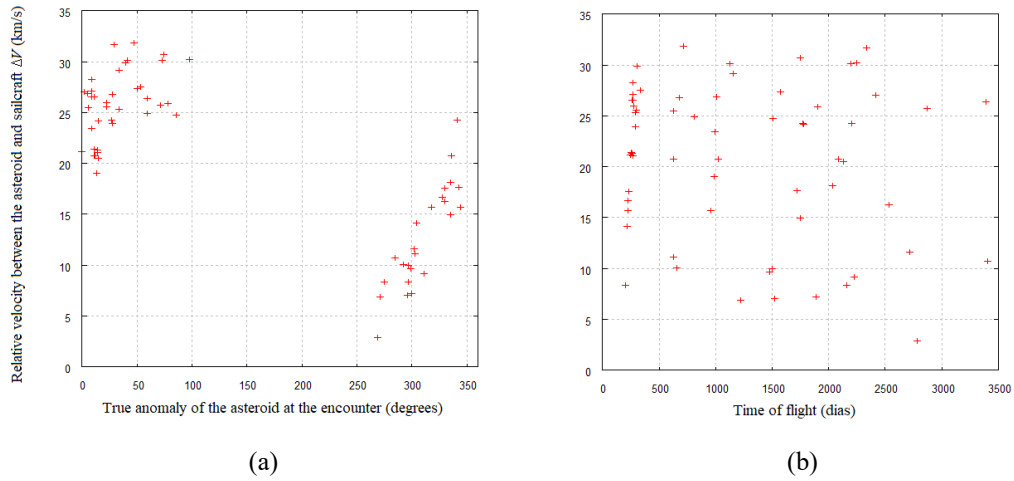


**Figure 8.**(a) Options of encounters as a function of the true anomaly of the asteroid at the encounter point. (b) Options as a function of the time of flight.

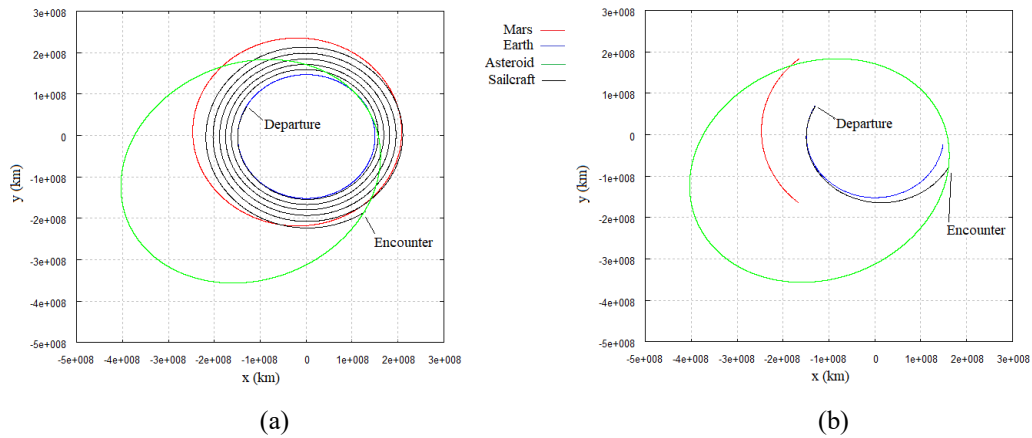


**Figure 9.** (a) trajectory with the smallest  $\Delta V = 2.842$  km/s,  $\Delta\theta = 1.543^\circ$ ,  $\Delta R_{PA} = 102$  km and time of flight of 2780,76 days (b) the fastest trajectory with time of flight of 205.79 days,  $\Delta V = 8.334$  km/s,  $\Delta\theta = 11.573^\circ$ ,  $\Delta R_{PA} = 117$  km.

### Acceleration analysis

It is considered an orbiting body subjected to an impulsive force that gives an extra acceleration  $\vec{a}$  to it. The time derivative of its specific orbital energy  $\dot{E}$  is given by  $\dot{E} = \vec{v} \cdot \vec{a}$  and its specific angular momentum  $\dot{h}$  is given by  $\dot{h} = \vec{r} \times \vec{a}$ , where  $\vec{r}$  is the body's position vector and  $\vec{v}$  its velocity

vector. It is also possible to get the variation over time of the semi-major axis ( $\dot{a}$ ) and eccentricity ( $\dot{e}$ ) of the orbit of the sailcraft, which are given by  $\dot{a} = \frac{2}{\mu} \dot{E} a^2$  and  $\dot{e} = \frac{1}{2ae} \left[ \dot{a}(1 - e^2) - \frac{2\dot{h}h}{\mu} \right]$ , where  $a$  is the semi-major axis of the orbit of the sailcraft,  $e$  is its eccentricity,  $h$  is its specific angular momentum and  $\mu$  the standard gravitational parameter of the orbital system. It is also possible to determine the variation over the time of the pericenter of the orbit ( $\dot{r}_p$ ), which is given by  $\dot{r}_p = \dot{a}(1 - e) - a\dot{e}$ .

To perform numerical simulations, it is considered a body orbiting the Sun with an initial orbit with semi-major axis of 2 A.U. and eccentricity 0.5, with an impulsive acceleration of 1 mm/s<sup>2</sup> acting over it. It is also possible to consider some dependencies between the perihelion variation, the angle between the direction of the acceleration and the direction of the trajectory of the body and the initial location of the orbit where the impulsive acceleration is applied.

The angle between the direction of the acceleration and the orbit's circumferential direction is called here  $\gamma_c$ , as shown in Figure 10. This figure shows  $\dot{r}_p$  as a function of both  $\gamma_c$  and the initial true anomaly of the body. The blue line indicates the maximum  $\dot{r}_p$  as a function of the true anomaly. Figure 11 also shows the angle between the direction of the acceleration and the orbit's tangential direction ( $\gamma$ ) of these maximum  $\dot{r}_p$ .

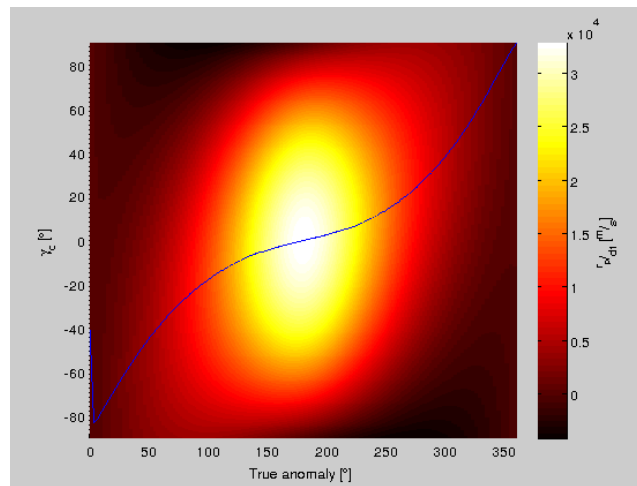


**Figure 10. Variation sensitivity of the periapsis of the asteroid.**

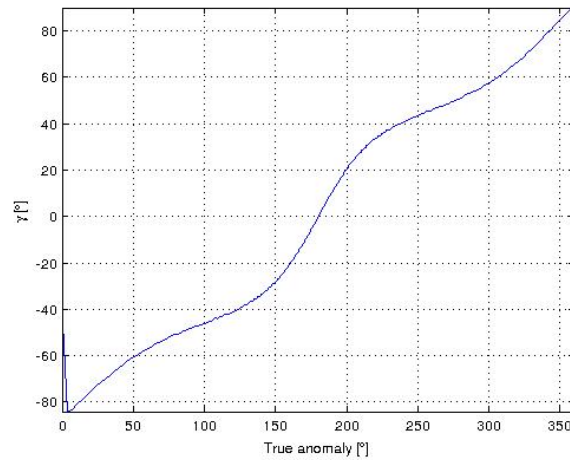


**Figure 11. Values of  $\gamma$  for maximum  $dr_p/dt$ .**

A square solar sail with mass of 20 kg and area of 2,193 m<sup>2</sup>, which is able to offer an acceleration of 1 mm/s<sup>2</sup> at the distance of 1 A.U., was used for these simulations. A series of four strategies were adopted to generate four types of trajectories for the sailcraft. For each strategy, the initial position of the Earth, and consequently the sailcraft, were located at the heliocentric true anomalies of 0, 45, 90, 135, 180, 225, 270 and 315 degrees. The strategies consisted of trajectories that: i) keep  $\alpha = 35^\circ$  until the collision; ii) change  $\alpha$  to perform two Solar flybys before the collision; iii) change  $\alpha$  to perform 3 Solar flybys before the collision; iv) changes  $\alpha$  to perform 3 Solar flybys, even closer than the ones used in the previous strategy. This strategy had to limit the spacecraft approximation for the flybys, which cannot go above the sailcraft's operational limit of 0.1 A.U..

The collision was considered perfectly inelastic, between two bodies with masses of 20 kg and  $2.7 \times 10^{10}$  kg, considering a sailcraft and the asteroid Apophis, respectively. The new state vectors were then used to determine the new orbital parameters and, consequently, the increase in the perihelion distance or, in other words, the increase in the distance between the new orbit of the asteroid and the circular orbit of the Earth.

The increased values of the perihelion distance for the new orbit, as well as the magnitude of the difference in velocities between the spacecraft and the asteroid in the moment of the collision, are presented in Figure 12 for each of the different strategies and initial position used in the simulations. The trajectories that provide the largest increases for each strategy are presented in Fig. 13.

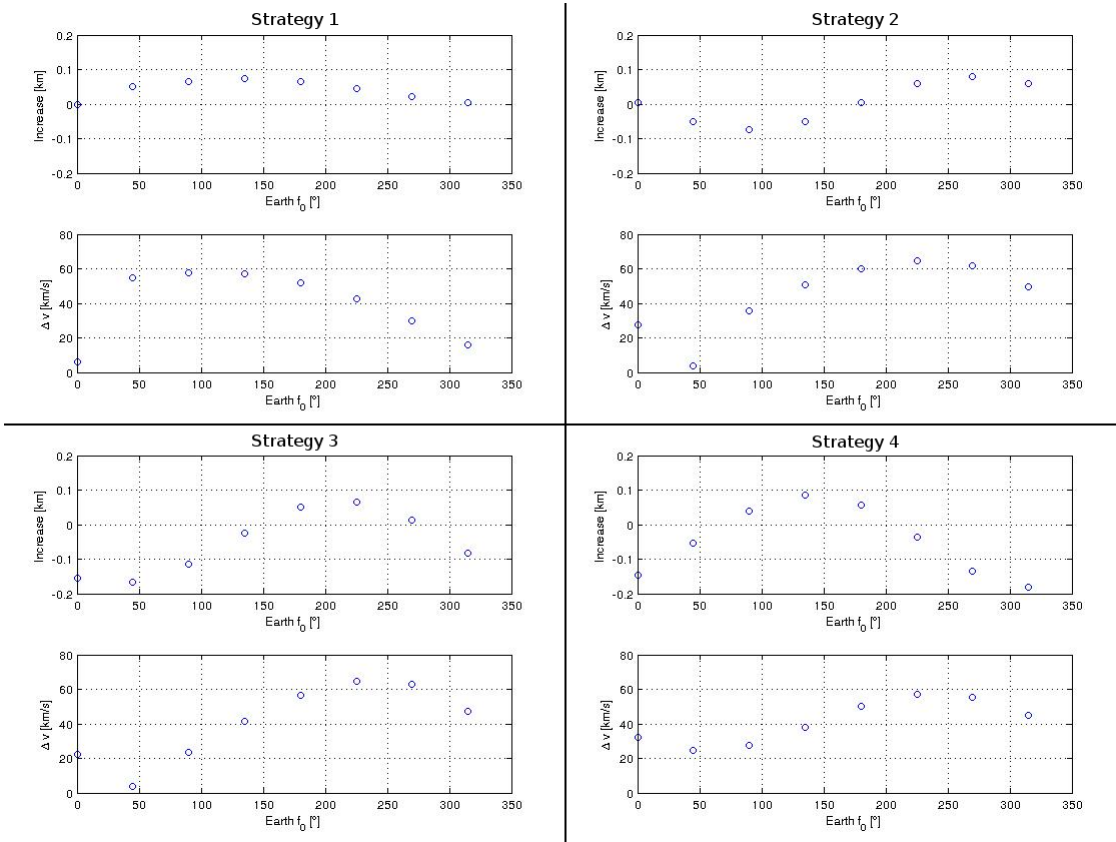
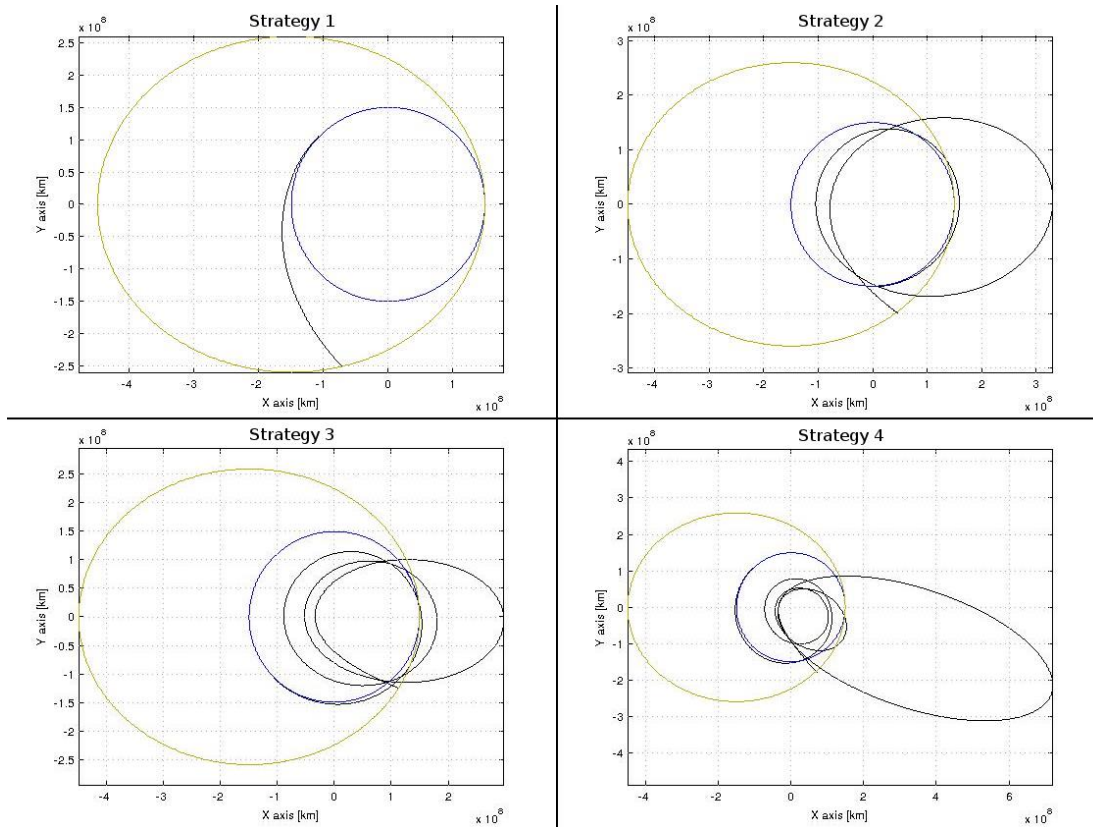


Figure 12. Perihelion increases and  $\Delta v$  at collisions for the four strategies used.



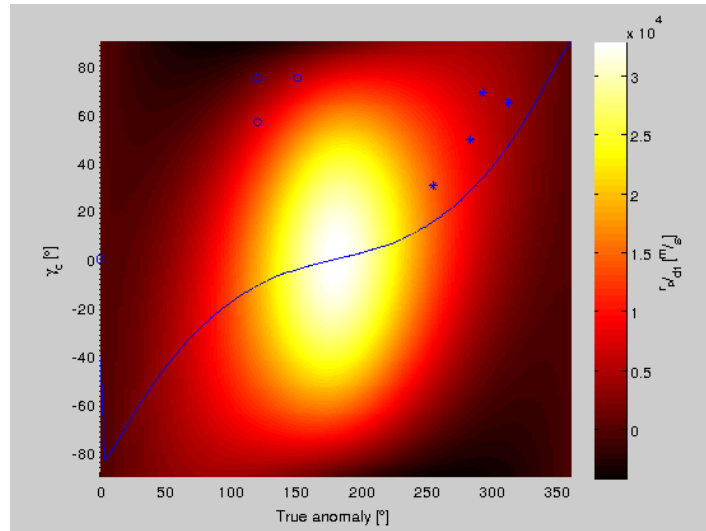
**Figure 13 - Trajectories for the sailcraft.**

Figure 13 shows the trajectories identified in Figure 12 with respect to their true anomaly and  $\gamma_C$  at the moment of the collision. This relation is shown in Figure 14. The trajectories with the largest increase in the perihelion distance, for each strategy, are indicated by a ‘\*’ sign, while the trajectories with the lowest increase (or greatest decrease), for each strategy, are indicated by a ‘o’ sign.

It is easy to notice that the trajectories with the greatest increase are the ones closer to the maximum  $r_p$  blue line, which is to be expected. It is important to remember that  $r_p$  is also dependent on the magnitude of the impulsive acceleration. This fact is emphasized because the analysis made in Figure 10 is made by using the same acceleration. Every trajectory simulated has a different acceleration produced by its collision. As a result, the magnitude of the perihelion increase cannot be objectively analyzed over the Z axis of Figure 14, being only interesting to make an analysis over the XY plane, as done here.

A second consideration to be made is the lack of necessity to develop a complex trajectory for the collision. Each strategy was planned such that the spacecraft had increasingly more specific orbital energy at the moment of the impact. However, there was no significant increase in the perihelion variation between the different strategies. This shows the strong dependency that this problem has with the “ $\gamma$  - true anomaly” pair, along with the great influence of the mass of the spacecraft colliding with the asteroid.

A third and final note, closely related to the one presented in the previous paragraph, is that not necessarily a greater  $\Delta v$  at the moment of collision yields a larger perihelion increase. Large  $\Delta v$  values are related to greater  $\gamma$  and, as seen, larger  $\gamma$  do not necessarily offer the larger  $r_p$ .



**Figure 14. Trajectories' perihelion sensitivity.**

## CONCLUSION

The goal of the present paper was to find trajectories for a spacecraft to reach asteroids using a solar sail as a propulsion system, to save fuel consumption. The idea is to identify trajectories mapping their main elements, such that the relative velocities between the spacecraft and the asteroid, the angle of collision, etc. Those data can be used to design any type of mission to asteroids, including scientific/technological missions, collision avoidance and missions with the goal of mining the asteroid.

Every time that a collision is detected between the sailcraft and the asteroid, it is also measured the asteroid velocity, the specific angular momentum, and the semi-major axis and eccentricity of the orbit, as well as the deviation of the perihelion of the orbit of the asteroid. Those elements are very important to know the effects of the collision in terms of deviating the trajectory of the asteroid, which is one of the main reasons to travel to an asteroid nowadays.

The results showed that the lowest relative velocities between the sailcraft and the asteroid, which is important for a rendezvous mission occur, for the majority of the cases, for true anomalies of the asteroid in the 3rd and 4th quadrants. Those are the regions where the angle between their velocities are small.

When considering missions to impact and deviate the asteroid, the best results are also usually with the true anomaly of the asteroid in the 3th and 4th quadrants, but the encounters have to occur far from the perihelion of the orbit of the asteroid around the Sun. Therefore, the most important aspect is that the sailcraft approaches the asteroid with the smallest possible angle between their velocities and as far away as possible from the perihelion of the asteroid.

It was also found that not necessarily a large variation of velocity at the moment of the collision yields a larger increase in the variation of the perihelion of the asteroid, because larger variations of velocity are related to larger  $\gamma$  and larger  $\gamma$  do not necessarily offer the larger time derivatives of the perihelion position.

The results also showed the importance of the initial position of the spacecraft when starting the use of the solar sail, as well as its mass.

## ACKNOWLEDGMENTS

The authors wish to express their appreciation for the support provided by grants #406841/2016-0, 301338/2016-7 from the National Council for Scientific and Technological Development (CNPq); grants #2016/15675-1, 2016/14665-2, from São Paulo Research Foundation (FAPESP) and the financial support from the National Council for Scientific and Technological Development (CNPq).

## REFERENCES

- <sup>1</sup> Baoyin, H., and Li, J. F., “A Survey on Orbital Dynamics and Navigation of Asteroid Missions,” *Acta Mechanica Sinica*, Vol. 30, No. 3, 2014, pp. 282–293. doi:10.1007/s10409-014-0035-8.
  - <sup>2</sup> Zelenyi, L. and Ksanfomality, L., “From the Vega mission to comet Halley to the Rosetta mission to comet 67/P Churyumov-Gerasimenko.” *Solar System Research*, 2016, Vol.50 (7), p.451-464.
  - <sup>3</sup> Andrews, D.G.; Bonner, K.D.; Butterworth, A.W.; Calvert, H.R.; Dagang, B.R.H.; Dimond, K.J.; Eckenroth, L.G.; Erickson, J.M.; Gilbertson, B.A.; Gompertz, N.R.; Igbinosun, O.J.; Ip, T.J.; Khan, B.H.; Marquez, S.L.; Neilson, N.M.; Parker, C.O.; Ransom, E.H.; Reeve, B.W.; Robinson, T.L.; Rogers, M.; Schuh, P.M.; Tom, C.J.; Wall, S.E.; Watanabe, N.; Yoo, C.J., “Defining a successful commercial asteroid mining program”, *Acta Astronautica*, March-April 2015, Vol.108, pp.106-118.
  - <sup>4</sup> Gates, M.; Stich, S.; McDonald, M.; Muirhead, B.; Mazanek, D.; Abell, P.; Lopez, P.; “The Asteroid Redirect Mission and sustainable human exploration”. *Acta Astronautica*, 2015, Vol. 111, p. 29-36.
  - <sup>5</sup> McInnes, C. R., “Solar Sailing: Technology, Dynamics and Mission Applications”. 2. ed. United Kingdom: Springer and Praxis Publishing, 2004.
  - <sup>6</sup> Tsuda, Y.; Mori, O.; Funase, R.; Sawada, H.; Yamamoto, T.; Saiki, T.; Endo, T.; Yonekura, K.; Hoshino, H.; Kawaguchi, J.; “Achievement of IKAROS — Japanese deep space solar sail demonstration mission”, *Acta Astronautica*, (2013), Vol.82, Issue 2, p. 183-188.
  - <sup>7</sup> Dachwald, B.; Sebaldt, W.; “Multiple near-Earth asteroid rendezvous and sample return using 1st generation solar sailcraft”. *Acta Astronautica*, v. 57, p. 864-875, 2005.
  - <sup>8</sup> Dachwald, B.; Sebaldt, W.; Richter, L.; “Multiple rendezvous and sample return missions to near-Earth objects using solar sailcraft”. *Acta Astronautica*, v. 59, p. 768 -776, 2006.
  - <sup>9</sup> Pereira, M. C. “Dinâmica Orbital e controle de orientação de um veículo especial com uma vela solar composta”. Doctoral Dissertation. 2009. Instituto Nacional de Pesquisas Espaciais, São José dos Campos, SP, Brazil.
  - <sup>10</sup> Wie, B. “Solar sail attitude control and dynamics, part 1”. *Journal of Guidance, Control, and Dynamics*, v. 27, n.4, p. 526 - 535, 2004.
  - <sup>11</sup> Vulpetti G.; Johnson, L.; Matloff, G. L.; “Solar Sails: a novel approach to interplanetary travel”, 2015, 2nd edition, New York: Copernicus Books 2015 277 p.
  - <sup>12</sup> Carrara, V. “Modelagem das forças e torques atuantes em satélites”. Master Thesis. 1982. Instituto Nacional de Pesquisas Espaciais, São José dos Campos, SP, Brazil.
- Macdonald, M. “Advances in Solar Sailing” Springer Praxis Boucks – Astronautical Engineering, 2014. Chichester, UK,